Structure of the inositol 1,4,5-trisphosphate receptor binding core in complex with its ligand

Ivan Bosanac*, Jean-René Alattia*, Tapas K. Mal*, Jenny Chan*, Susanna Talarico*, Frances K. Tong*, Kit I. Tong*, Fumio Yoshikawa†, Teiichi Furuichi†, Miwako Iwai‡, Takayuki Michikawa‡§, Katsuhiko Mikoshiba†‡§ & Mitsuhiko Ikura*

* *Division of Molecular and Structural Biology, Ontario Cancer Institute and Department of Medical Biophysics, University of Toronto, 610 University Avenue, Toronto, Ontario, Canada M5G 2M9*
† *Laboratory for Developmental Neurobiology and Molecular Neurogenesis, Brain Science Institute, RIKEN, Saitama 351-0198, Japan*
‡ *Department of Molecular Neurobiology, Institute of Medical Science, University of Tokyo, Tokyo 108-8639, Japan*
§ *Calcium Oscillation Project, ICORP, Japan Science and Technology Corporation (JST), Tokyo, 108-0071, Japan*

In a variety of cells, the Ca^{2+} signalling process is mediated by the endoplasmic-reticulum-membrane-associated Ca^{2+} release channel, inositol 1,4,5-trisphosphate ($InsP_3$) receptor ($InsP_3R$)[1]. Being ubiquitous and present in organisms ranging from humans to *Caenorhabditis elegans*, $InsP_3R$ has a vital role in the control of cellular and physiological processes as diverse as cell division, cell proliferation, apoptosis, fertilization, development, behaviour, memory and learning[2]. Mouse type I $InsP_3R$ ($InsP_3R1$), found in high abundance in cerebellar Purkinje cells, is a polypeptide with three major functionally distinct regions: the amino-terminal $InsP_3$-binding region, the central modulatory region and the carboxy-terminal channel region[2]. Here we present a 2.2-Å crystal structure of the $InsP_3$-binding core of mouse $InsP_3R1$ in complex with $InsP_3$. The asymmetric, boomerang-like structure consists of an N-terminal β-trefoil domain and a C-terminal α-helical domain containing an 'armadillo repeat'-like fold. The cleft formed by the two domains exposes a cluster of arginine and lysine residues that coordinate the three phosphoryl groups of $InsP_3$. Putative Ca^{2+}-binding sites are identified in two separate locations within the $InsP_3$-binding core.

The recombinant construct encoding only residues 224–604 of mouse $InsP_3R1$ ($InsP_3R1_c$; Fig. 1) binds $InsP_3$ with high affinity ($K_d \approx 0.09$ nM)[3]. The crystal structure of mouse $InsP_3R1_c$ reveals that the protein forms an elongated L-shaped structure with two asymmetric domains oriented perpendicularly to each other (Fig. 2a). The N-terminal domain (residues 224–436) is composed of 12 β-strands and 2 single-turn helices, forming a globular barrel with approximate dimensions $35 \times 40 \times 30$ Å^3 (Fig. 2a). In contrast, the C-terminal portion of mouse $InsP_3R1_c$ (residues 437–604) consists of eight α-helices, forming a bundle with dimensions $34 \times 26 \times 30$ Å^3 (Fig. 2a). At the interface of these structurally distinct domains, hereafter referred to as the β-domain and the α-domain respectively, resides a deep cleft lined with basic residues. These residues are responsible for anchoring $InsP_3$ to the receptor (Fig. 2d), in a manner totally different from the phosphoinositides-binding modes observed in the pleckstrin homology (PH), ENTH (for 'epsin N-terminal homologue'), Tubby and FERM (for 'band 4.1, ezrin, radixin and moesin') domains[4,5]. The conformation of

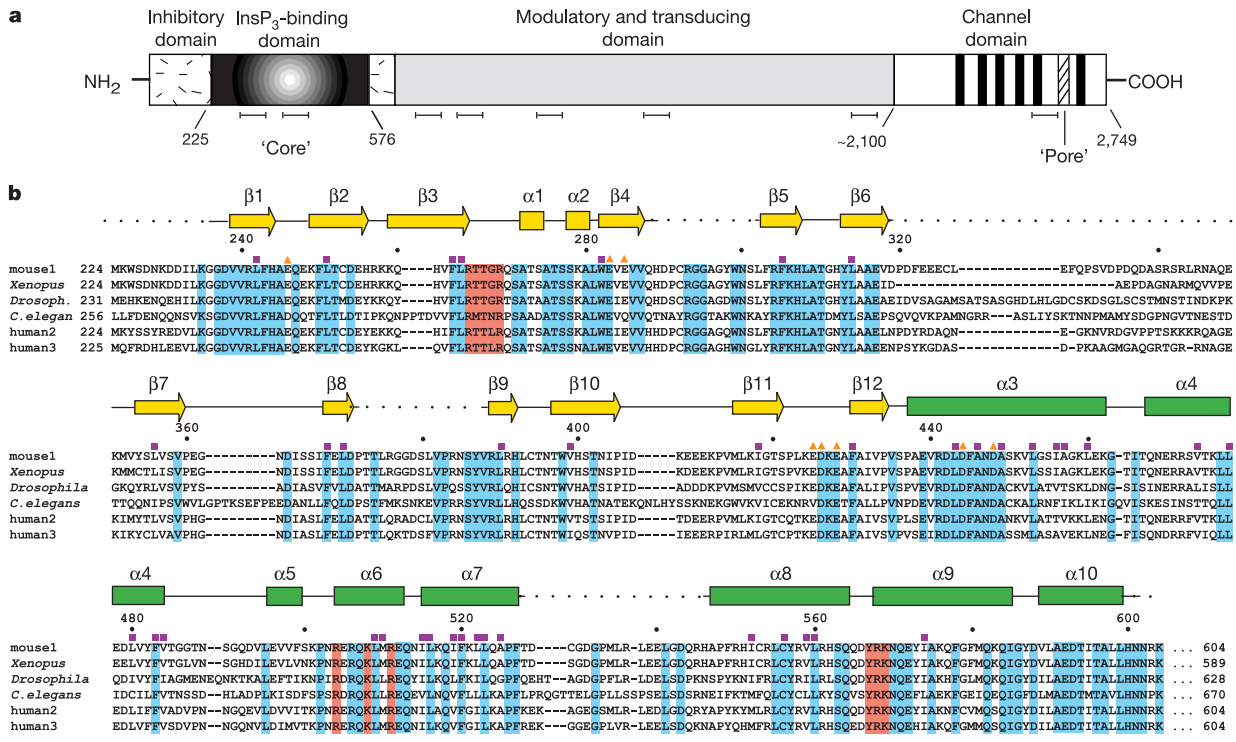

Figure 1 Overall domain architecture of $InsP_3R$ and sequence alignment of the $InsP_3$-binding core between members of the $InsP_3R$ family. **a**, The four functional domains of $InsP_3R1$ with Ca^{2+}-binding sites (horizontal bars), putative membrane-spanning segments (vertical solid bars) and pore-forming region (diagonally striped box). **b**, Sequence alignment of the $InsP_3$-binding core of $InsP_3Rs$: blue, conserved residues; red, $InsP_3$-coordinating residues; purple squares, hydrophobic core residues; orange triangles, Ca^{2+}-binding residues. β-Strands (arrows), α-helices (bars) and unidentified portions (dotted lines) are shown. The β-domain and the α-domain are coloured yellow and green, respectively. National Center for Biotechnology Information (NCBI) accession numbers for sequences: mouse1, ACMSIT; *Xenopus*, A40743; *Drosophila*, CAB51853; *C. elegans*, CAB45862; human2, XP_006747; human3, Q14573.

the receptor-bound $InsP_3$ molecule is similar to that found in the crystal structures of isolated $InsP_3$ and $InsP_3$ bound to a PH domain[6,7]. However, the phosphorus–phosphorus distances differ between this study (8.4, 7.2 and 5.0 Å for P1/P4, P1/P5 and P4/P5 pairs) and others (8.1, 6.9 and 4.1 Å for isolated $InsP_3$, and 8.2, 7.2 and 4.3 Å for $InsP_3$ bound to the PH domain)[8], with P4 and P5 separation being significant.

The protein fold of the β-domain is known as the β-trefoil and is found in a number of diverse proteins, including interleukins-1β and 1α, fibroblast growth factors and mannose receptors[9]. Despite the low identity (14%) between mouse $InsP_3R1_c$ and the mannose-receptor β-trefoil, the structure of these two β-trefoil folds can be readily superimposed (root-mean-square deviation (r.m.s.d.) = 2.3 Å) (Fig. 3a). In the β-domain of mouse $InsP_3R1_c$, three of the six two-stranded hairpins (strand pairs β1 and β4, β5 and β8, β9 and β12) make up a barrel, and the other three (β2 and β3, β6 and β7, β10 and β11) are in a triangular array that caps the barrel, giving rise to a molecular arrangement with a pseudo-three-fold symmetry.

Structural comparison of the α-domain, with known folds using the DALI algorithm[10], revealed a high homology to the armadillo repeat fold found in β-catenin[11], importins[12] and adenomatous polyposis coli[13]. The α-domain can be superimposed on the three consecutive armadillo repeats of β-catenin[11] (r.m.s.d. = 3.3 Å). Generally, an armadillo repeat consists of three α-helices with short interhelical linkers. In mouse $InsP_3R1_c$, helices α3 and α4 correspond to the second and third helices of the first armadillo repeat, and α6, α7 and α8 constitute a perfect armadillo repeat 2 (Fig. 3b). The third repeat in mouse $InsP_3R1_c$ consists of α9 and α10 and lacks the third helix in the construct used for the present study. As a result, the position of α10 is disoriented relative to the canonical armadillo repeat. In the aforementioned proteins these armadillo repeats act as a protein–protein interaction motif[13]. In mouse $InsP_3R1_c$, the two relatively large, highly conserved surface areas are identified within the α-domain. One conserved surface (P-I) encompasses the amino-acid residues P502, F527, Y557, Q564, Q571, E572, A575, F578 and Q582 (Fig. 2d). The other conserved surface (P-II) contains a high proportion of charged amino acids: E283, V286, K306, Y313, R441, D444, F445, N447, D448 and R506 (Fig. 2e). These conserved regions rich in aromatic residues might serve as interaction sites for other parts of the receptor or unidentified cellular proteins. One obvious candidate for such a binding domain is the N-terminal $InsP_3$ binding suppressor domain (residues 1–225), which reduces the $InsP_3$-binding affinity of the core domain from 90 pM to 45 nM (ref. 3).

Two different sequence-based analyses were used to search for the potential presence of additional armadillo repeats extending downstream of the α-domain. First, secondary structure prediction with PHD[14] showed that the region spanning residues 460–1500 is predominantly α-helical. Second, mGenTHREADER[15] analysis uncovered matches for possible armadillo repeats in regions within residues 760–1740 at 'high' confidence levels (*E*-values between 0.002 and 0.007). Armadillo repeats of this length (~1,200 residues including residues 440–604) would provide a long arm with a length of ~200 Å and a diameter of 35 Å, potentially connecting the $InsP_3$-binding domain and the modulatory domain. This is consistent with a recent electron microscope analysis of native $InsP_3R1$, which showed a rod-like linker structure between the $InsP_3$-binding region and the transmembrane channel core[16,17].

Highly basic amino acid residues spanning the two domains are

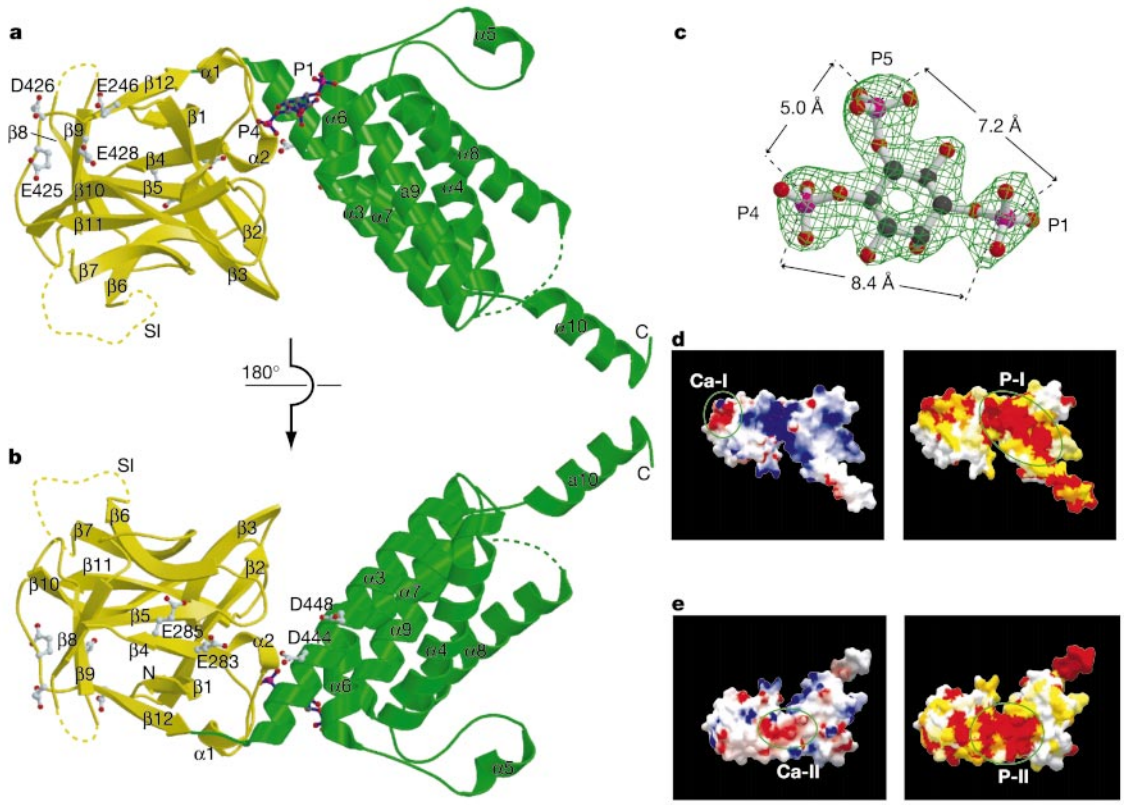

Figure 2 Structure of mouse $InsP_3R1_c$ in complex with $InsP_3$. **a**, The β-domain (yellow) and the α-domain (green) with the $InsP_3$ molecule at the interface. Residues in the Ca-I and Ca-II sites and the splicing site (SI) are shown. **b**, View in **a** rotated by 180°. **c**, Experimental MAD electron density map at 1.7σ around the $InsP_3$ molecule. **d**, **e**, Molecular surface representations of mouse $InsP_3R1_c$ in the same orientations as **a** and **b**, respectively. Surface electrostatic potential (left panel with Ca-I and Ca-II sites) and conserved surface residues (right panel with P-I, P-II sites; identical residues are shown in red, and least-conserved residues in white).

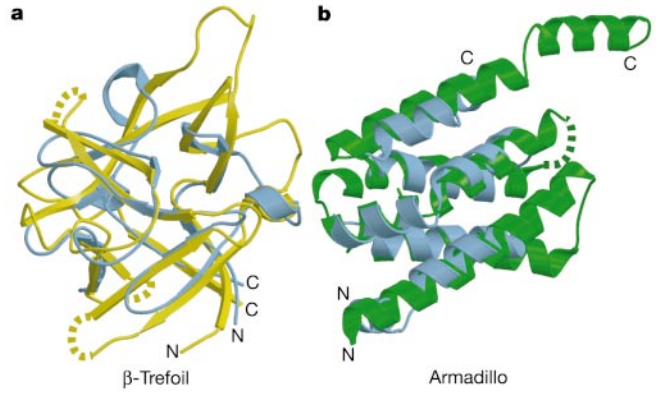

Figure 3 β-Trefoil and 'armadillo repeat'-like folds in mouse $InsP_3R1_c$. **a**, The β-domain (yellow) is superimposed on the cysteine-rich domain of the mannose receptor (blue) (accession number 1DQG, residues 4–128). The r.m.s.d. of the superposition is 2.3 Å. **b**, Superimposition of the α-domain (green) and β-catenin (blue) (accession number 3BCT, residues 269–368) with an r.m.s.d. of 3.3 Å. The size of one armadillo repeat of mouse $InsP_3R1_c$ is longer (a total of 62 amino acids in repeat 2) than those found in other proteins (typically 42 amino acids per repeat)[13].

responsible for the extensive interactions of $InsP_3$ with $InsP_3R$. In addition to the interactions between protein side chains and phosphorus, six water molecules are directly involved in the formation of hydrogen bonds that bridge $InsP_3$ and the receptor (Fig. 4c). The coordination of the P1 and P5 groups predominantly involves residues from the α-domain (Fig. 4a), whereas the P4 group anchors to mouse $InsP_3R1_c$ by means of hydrogen-bond interactions mediated by β-domain residues (Fig. 4b). P4 is involved in an extensive network of hydrogen bonds with residues R265, T266, T267, G268, R269 and K569. P5 also forms numerous hydrogen bonds with R265, R269, R504, K508, R511 and Y567. In contrast, P1 interacts only with R568 and K569 (Fig. 4). A less significant role for P1 has previously been suggested[18]. The hydroxyl groups of $InsP_3$ have a secondary role in binding to $InsP_3R$, which is consistent with earlier physico-chemical studies with monodeoxy, dideoxy and trideoxy derivatives of $InsP_3$ (ref. 19).

The current structure confirms the involvement of 9 out of 12 previously identified Arg/Lys residues as $InsP_3$-coordinating residues, whose mutations to Gln drastically reduce or abolish $InsP_3$-binding activity[20]. Exceptions are the three amino acids R241, K249 and R506. Residing outside the $InsP_3$-binding site, R241 in the β-domain forms a salt bridge with E439 in the α-domain, thereby stabilizing the inter-domain interaction. K249 and R506 are both located adjacent to the $InsP_3$-binding site and form salt bridges with T266 and D442, respectively, thereby contributing to the structural integrity of both α- and β-domains. The structure further reveals the involvement of non-basic residues T266, T267, G268 and Y567 in $InsP_3$ coordination. As a result, we constructed four additional mouse $InsP_3R1_c$ mutants carrying T266A, T267A, Y567F or Y567A (Fig. 4d). The mutant T266A showed very little effect on $InsP_3$ binding, which was consistent with $InsP_3$ coordination via the backbone carbonyl group rather than the side chain (Fig. 4). The last three mutants all showed a drastic reduction in $InsP_3$ binding, confirming the importance of the side-chain functional groups of T267 and Y567 in coordination with $InsP_3$.

Taylor and Marchant[21] have demonstrated the importance of a direct coupling between $InsP_3$ and Ca^{2+} binding to the cytoplasmic portion of $InsP_3R$ in the regulation of Ca^{2+} release channel activity. Previous truncation mutagenesis studies[22] identified two Ca^{2+}-binding fragments of $InsP_3R$, one encoding residues 304–381 and

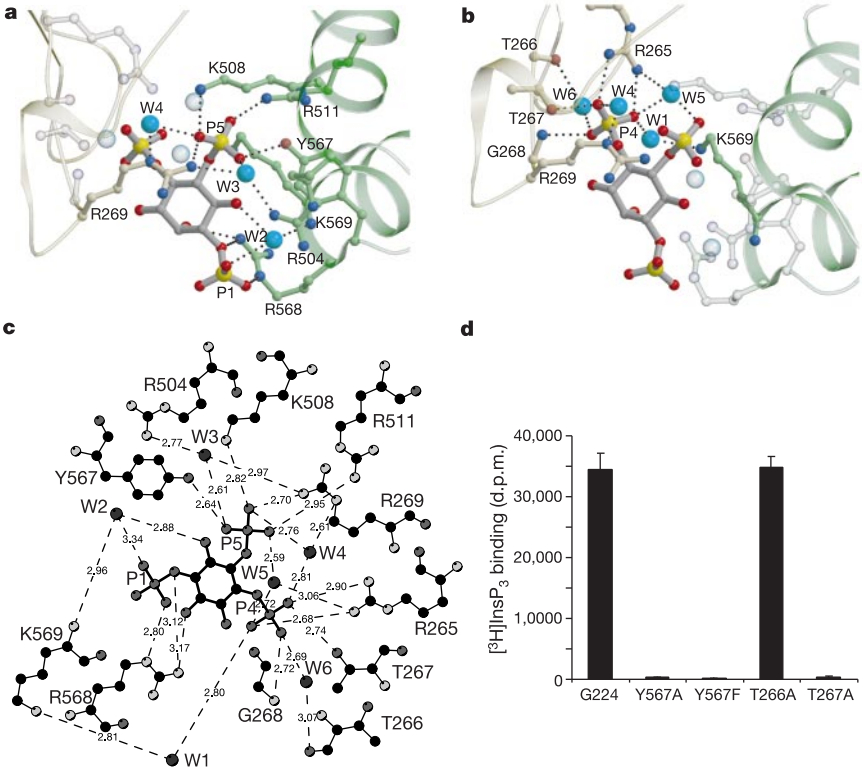

Figure 4 Coordination of $InsP_3$ by mouse $InsP_3R1_c$. Ribbon representation of the polypeptide chains of the α-domain (green) and the β-domain (yellow). Phosphates are shown in yellow, oxygens in red, nitrogens in blue, water molecules in cyan, and hydrogen bonds with dotted black lines. The coordination of P1 and P5 groups is shown in **a**, and that of P4 in **b**. **c**, Two-dimensional schematic representation of the interaction of mouse $InsP_3R1_c$ with $InsP_3$. **d**, Graph showing average specific $InsP_3$-binding activity of site-directed mutant from a minimum of four independent experiments.

the other corresponding to residues 378–450. More recently, residues E425, D426, E428, D442 and D444 have been shown to be essential for Ca^{2+} coordination[23]. These residues are part of the two surface acidic clusters identified in the present crystal structure of mouse $InsP_3R1_c$. The first site, Ca-I, is located in the β-domain and consists of residues E246, E425, D426 and E428 (Fig. 2d). The second site, Ca-II, located across the two domains, is composed of residues E283, E285, D444 and D448 (Fig. 2e). Interestingly, Ca^{2+}-binding site Ca-II overlaps with the conserved region P-II, suggesting that the binding of Ca^{2+} to this site is conformationally coupled with the aforementioned protein–protein interaction involving other protein domain(s). This finding, together with recent electron microscope studies of $InsP_3R$[16,17] and previous biochemical studies[21], leads to a tempting speculation on the Ca^{2+}–$InsP_3$ coupling mechanism required for channel activation. The role of binding of $InsP_3$ to the core domain (residues 226–576) might include the release of a conformational constraint that prevents Ca^{2+} from binding to the receptor. The N-terminal $InsP_3$ binding suppressor region (residues 1–225) might be directly involved in this negative regulation of Ca^{2+} binding to the receptor, in addition to the modulation of $InsP_3$ binding affinity[20]. It is equally possible that some other part of the $InsP_3R$ or an unidentified cellular protein is involved in this $InsP_3$–Ca^{2+} coupling mechanism. □

Methods

Overexpression and purification of $InsP_3R_c$

The mouse type 1 $InsP_3R$ protein fragment encompassing the ligand-binding core, residues 224–604, was expressed as a glutathione *S*-transferase (GST) fusion protein (GST–mouse $InsP_3R1_c$) by polymerase chain reaction, cloning and sequencing as described previously[20,24]. The protein was expressed in *Escherichia coli* strain BL21-CodonPlus-RIL (Stratagene) at 15 °C for ~20 h by induction with 0.5 mM isopropyl β-D-thiogalactopyranoside[24]. GST–mouse $InsP_3R1_c$ was first purified with glutathione–Sepharose (Pharmacia) followed by digestion overnight with thrombin to remove GST from the cutting buffer (20 mM Tris-HCl pH 8.4, 200 mM NaCl, 10% (v/v) glycerol and 20 mM dithiothreitol) at 4 °C with constant mixing. Cation-exchange chromatography (Fractogel EMD SO_3^- resin; EM Industries Inc.) and size-exclusion chromatography (Superdex 75; Pharmacia) were then performed to remove thrombin and any other impurities. Selenomethionine-labelled protein was produced by the technique involving the inhibition of methionine biosynthesis[25] and was confirmed by electrospray mass spectrometry. The purified protein was concentrated to 20 mg ml^{-1} in a crystallization buffer (15 mM Tris-HCl pH 8.0, 300 mM Na_2SO_4, 2 mM tris-(2-carboxyethyl)phosphine and 50% molar excess $InsP_3$).

Crystallization and data collection

Initial crystals of mouse $InsP_3R1_c$ were produced at 295 K by the hanging-drop method by adding 2 μl of protein complex to 2 μl of well solution (100 mM MES pH 6.0, 20% polyethylene glycol (PEG) 3350, 0.2 M CH_5NO_3 and 2–5% dioxane). Crystals of the complex grew as extensive clusters of rods within 2 weeks. Series of microseedings were required to obtain single rod-type crystals with dimensions of 0.05 × 0.1 × 0.4 mm^3. Crystals were flash-cooled in crystallization buffer supplemented with 25% PEG 400. Multiwavelength anomalous dispersion (MAD) and native data were collected at 100 K on a BL44XU beam line at the SPring-8 Synchrotron facility and were processed with d*TREK[26]. Crystals belonged to space group $C222_1$ with cell dimensions $a = 44.2$ Å, $b = 90.3$ Å and $c = 207.9$ Å, and contained one complex in the asymmetric unit. Radiation damage to the crystal prevented completion of the data set at λ_3 (remote wavelength) (Supplementary Table 1).

Structure determination and refinement

The initial positions of four out of six expected selenium atoms were determined by Solve[27] and refined with SHARP[28] to a figure of merit of 0.42. The position of the two missing selenomethionine residues (M224 and M535) were never identified because one is located at the N terminus of the protein fragment and the other in the α7/α8 loop region, which is not visible in the present model. Density modification and solvent flattening with the program CNS[29] increased the overall figure of merit to 0.93. The experimental map had continuous electron density for most of mouse $InsP_3R1_c$; the $InsP_3$ ligand was easily identifiable. Model building was performed with the program O[30] and refinement with CNS[29]. The final model contained residues 236–288, 302–319, 351–372, 387–528 and 546–602, with 92.7% of residues in the most favoured regions of the Ramachandran plot and no residues in the disallowed region. The β-domain contains three crystallographically invisible loops, between strands β4/β5, β6/β7 and β8/β9 with the loop encompassing residues 320 to 350 (β6/β7) having a splicing site I. In total, 2,522 atoms with a mean temperature factor at 34.1 Å^2 were observed: 2,356 protein atoms ($\langle B \rangle = 35.2$ Å^2), 24 ligand atoms ($\langle B \rangle = 28.6$ Å^2) and 142 solvent atoms ($\langle B \rangle = 36.2$ Å^2). The R_{cryst} and R_{free} of the final model were 22.4 and 25.0, respectively.

$InsP_3$ binding assay

Site-directed mutagenesis of Y567A, Y567F, T266A and T267A was introduced into mouse $InsP_3R1_c$, and protein fragments were expressed in *E. coli*. Preparation of soluble protein from the cell pellets was performed as described elsewhere[24]. Soluble protein (30 μg) was diluted to 100 μl with the binding buffer and incubated with 9.6 nM [^{3}H]$InsP_3$ for 10 min at 4 °C in the absence and presence of 10 μM $InsP_3$ to measure total and nonspecific binding, respectively. After the addition of 4 μl of 50 mg ml^{-1} γ-globulin and 100 μl of a solution containing 30% (w/v) PEG 6000, 1 mM EDTA and 50 mM Tris-HCl (pH 8.0 at 4 °C), the $InsP_3$–protein mixture was incubated for a further 5 min at 4 °C. The protein–PEG complex was pelleted by centrifugation at 18,000*g* for 5 min at 4 °C. The resultant pellet was solubilized with 180 μl of Solvable (Packard), then neutralized by the addition of 18 μl of acetic acid. After mixing 5 ml of Atomlight (Packard), radioactivity of the samples was measured with a liquid-scintillation counter (Beckman). Specific binding activity was defined by subtracting nonspecific binding from total binding.

Received 15 August; accepted 29 October 2002; doi:10.1038/nature01268.
Published online 17 November 2002.

1. Berridge, M. J., Lipp, P. & Bootman, M. D. The versatility and universality of calcium signalling. *Nature Rev. Mol. Cell Biol.* **1,** 11–21 (2000).
2. Furuichi, T. & Mikoshiba, K. Inositol 1,4,5-trisphosphate receptor-mediated Ca^{2+} signaling in the brain. *J. Neurochem.* **64,** 953–960 (1995).
3. Uchiyama, T., Yoshikawa, F., Hishida, A., Furuichi, T. & Mikoshiba, K. A novel recombinant hyperaffinity inositol 1,4,5-trisphosphate (IP_3) absorbent traps IP_3, resulting in specific inhibition of IP_3-mediated calcium signaling. *J. Biol. Chem.* **277,** 8106–8113 (2002).
4. Overduin, M., Cheever, M. L. & Kutateladze, T. G. Signaling with phoshoinositides: better than binary. *Mol. Interventions* **1,** 151–159 (2001).
5. Hamada, K., Shimizu, T., Matsui, T., Tsukita, S. & Hakoshima, T. Structural basis of the membrane-targeting and unmasking mechanisms of the radixin FERM domain. *EMBO J.* **19,** 4449–4462 (2000).
6. Ferguson, K. M., Lemmon, M. A., Schlessinger, J. & Sigler, P. B. Structure of the high affinity complex of inositol trisphosphate with a phospholipase C pleckstrin homology domain. *Cell* **83,** 1037–1046 (1995).
7. Hyvonen, M. *et al.* Structure of the binding site for inositol phosphates in a PH domain. *EMBO J.* **14,** 4676–4685 (1995).
8. Hotoda, H. *et al.* Molecular recognition of adenophostin, a very potent Ca^{2+} inducer, at the D-*myo*-inositol 1,4,5-trisphosphate receptor. *Biochemistry* **38,** 9234–9241 (1999).
9. Murzin, A. G., Lesk, A. M. & Chothia, C. beta-Trefoil fold. Patterns of structure and sequence in the Kunitz inhibitors interleukins-1β and 1α and fibroblast growth factors. *J. Mol. Biol.* **223,** 531–543 (1992).
10. Holm, L. & Sander, C. Protein structure comparison by alignment of distance matrices. *J. Mol. Biol.* **233,** 123–138 (1993).
11. Huber, A. H., Nelson, W. J. & Weis, W. I. Three-dimensional structure of the armadillo repeat region of β-catenin. *Cell* **90,** 871–882 (1997).
12. Cingolani, G., Petosa, C., Weis, K. & Muller, C. W. Structure of importin-β bound to the IBB domain of importin-α. *Nature* **399,** 221–229 (1999).
13. Peifer, M., Berg, S. & Reynolds, A. B. A repeating amino acid motif shared by proteins with diverse cellular roles. *Cell* **76,** 789–791 (1994).
14. Rost, B., Sander, C. & Schneider, R. PHD—an automatic mail server for protein secondary structure prediction. *Comput. Appl. Biosci.* **10,** 53–60 (1994).
15. Jones, D. T. GenTHREADER: an efficient and reliable protein fold recognition method for genomic sequences. *J. Mol. Biol.* **287,** 797–815 (1999).
16. Hamada, K., Miyata, T., Mayanagi, K., Hirota, J. & Mikoshiba, K. Two-state conformational changes in inositol 1,4,5-trisphosphate receptor regulated by calcium. *J. Biol. Chem.* **277,** 21115–21118 (2002).
17. Jiang, Q. X., Thrower, E. C., Chester, D. W., Ehrlich, B. E. & Sigworth, F. J. Three-dimensional structure of the type 1 inositol 1,4,5-trisphosphate receptor at 24 Å resolution. *EMBO J.* **21,** 3575–3581 (2002).
18. Wilcox, R. A., Primrose, W. U., Nahorski, S. R. & Challiss, R. A. New developments in the molecular pharmacology of the *myo*-inositol 1,4,5-trisphosphate receptor. *Trends Pharmacol. Sci.* **19,** 467–475 (1998).
19. Kozikowski, A. P., Ognyanov, V. I., Fauq, A. H., Nahorski, A. R. & Wilcox, R. A. Synthesis of 1D-3-deoxy-, 1D-2,3-dideoxy-, and 1D-2,3,6-trideoxy-myo-inositol 1,4,5-trisphosphate from quebrachitol, their binding affinities, and calcium release activity. *J. Am. Chem. Soc.* **115,** 4429–4434 (1993).
20. Yoshikawa, F. *et al.* Mutational analysis of the ligand binding site of the inositol 1,4,5-trisphosphate receptor. *J. Biol. Chem.* **271,** 18277–18284 (1996).
21. Marchant, J. S. & Taylor, C. W. Cooperative activation of IP_3 receptors by sequential binding of IP_3 and Ca^{2+} safeguards against spontaneous activity. *Curr. Biol.* **7,** 510–518 (1997).
22. Sienaert, I. *et al.* Molecular and functional evidence for multiple Ca^{2+}-binding domains in the type 1 inositol 1,4,5-trisphosphate receptor. *J. Biol. Chem.* **272,** 25899–25906 (1997).
23. Sienaert, I. *et al.* Localization and function of a calmodulin/apocalmodulin binding domain in the N-terminal part of the type 1 inositol 1,4,5-trisphosphate receptor. *Biochem. J.* **365,** 269–277 (2002).
24. Yoshikawa, F. *et al.* High efficient expression of the functional ligand binding site of the inositol 1,4,5-triphosphate receptor in *Escherichia coli*. *Biochem. Biophys. Res. Commun.* **257,** 792–797 (1999).
25. Van Duyne, G. D., Standaert, R. F., Karplus, P. A., Schreiber, S. L. & Clardy, J. Atomic structures of the human immunophilin FKBP-12 complexes with FK506 and rapamycin. *J. Mol. Biol.* **229,** 105–124 (1993).
26. Pflugrath, J. W. The finer things in X-ray diffraction data collection. *Acta Crystallogr. D* **55,** 1718–1725 (1999).
27. Terwilliger, T. C., Kim, S. H. & Eisenberg, J. Generalized method of determining heavy-atom positions using the difference Patterson function. *Acta Crystallogr. A* **43,** 1–5 (1987).
28. La Fortelle, E. D. & Bricogne, G. Maximum-likelihood heavy atom parameter refinement in the MIR and MAD methods. *Methods Enzymol.* **276,** 472–494 (1997).
29. Brunger, A. T. *et al.* Crystallography and NMR system: A new software suite for macromolecular structure determination. *Acta Crystallogr. D* **54,** 905–921 (1998).
30. Jones, T. A., Zou, J. Y., Cowan, S. W. & Kjeldgaard, M. Improved methods for binding protein models

in electron density maps and the location of errors in these models. *Acta Crystallogr. A* **47,** 110–119 (1991).

Supplementary Information accompanies the paper on *Nature*'s website (**http://www.nature.com/nature**).

Acknowledgements We thank A. Nakagawa, A. Miyazaki and K.T. Chong for their assistance at the beamline BL44XU at SPring-8, Japan; the staff at the X8-C and X25 beamline of Brookhaven National Laboratory and the BioCars beamline at Advanced Photon Source for their assistance; D. Jones and M. Swindells for mGenTHREADER analysis; and members of our division for discussions. This work was supported by grants from the Canadian Institutes of Health Research (CIHR) to I.B. and M.I., and by grants from RIKEN (to K.M.) and the Ministry of Education, Science, Sports, and Culture of Japan (to K.M. and T.M.). M.I. is a CIHR Investigator.

Competing interests statement The authors declare that they have no competing financial interests.

Correspondence and requests for materials should be addressed to M.I. (e-mail: mikura@uhnres.utoronto.ca). The atomic coordinates for $InsP_3$-bound mouse $InsP_3R1_c$ have been deposited in the Protein Data Bank under accession code 1N4K.

erratum

The strength of $Mg_{0.9}Fe_{0.1}SiO_3$ perovskite at high pressure and temperature

Jiuhua Chen, Donald J. Weldner & Michael T. Vaughan

Nature **419**, 824–826 (2002).

On page 825 of this Letter, the equation should not have contained 'kern +1' in the second term. The equation should read:

$$\mathrm{FWHM}^2 = (2\varepsilon E)^3 + (Khc/2P\sin\theta_0)^2$$

□

